Energy Economics 124 (2023) 106773

Contents lists available at ScienceDirect

Energy Economics

journal homepage: www.elsevier.com/locate/eneeco

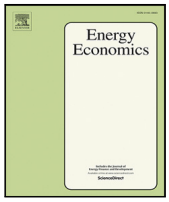

Green investment and asset stranding under transition scenario uncertainty

Maria Flora [a,1], Peter Tankov [b,*]

[a] CREST, CNRS, IP Paris, 5 avenue Henry Le Chatelier, 91120 Palaiseau, France
[b] CREST, ENSAE, IP Paris, 5 avenue Henry Le Chatelier, 91120, Palaiseau, France

ARTICLE INFO

Dataset link: www.macrobond.com, https://data.ene.iiasa.ac.at/ngfs, https://github.com/petertankov/green-invest

JEL classification:
Q42
Q51

Keywords:
Transition risk
Scenario uncertainty
Bayesian learning
Stranded asset
Real options

ABSTRACT

Risks and opportunities related to environmental transition are usually evaluated through the use of scenarios, produced and maintained by international bodies such as the International Energy Agency. This approach assumes perfect knowledge of the scenario by the agent, but in reality, scenario uncertainty is an important obstacle for making optimal investment or divestment decisions. In this paper, we develop a real-options approach to evaluate assets and potential investment projects under dynamic climate transition scenario uncertainty. We use off-the-shelf Integrated Assessment Model (IAM) scenarios and assume that the economic agent acquires the information about the scenario progressively by observing a signal, such as the carbon price or the greenhouse gas emissions. The problem of valuing an investment is formulated as an American option pricing problem, where the optimal exercise time corresponds to the time of entering a potential investment project or the time of selling a potentially stranded asset. To illustrate our approach, we employ representative scenarios from the scenario database of the Network for Greening the Financial System in two energy-related examples: the divestment decision from a coal-fired power plant without Carbon Capture and Storage (CCS) technology and the potential investment into a green coal-fired power plant with CCS. In both cases, we find that the real option value is very sensitive to scenario uncertainty: the value of the coal-fired power plant is reduced by 25% and that of the green coal investment project is reduced by 7% when the agent deduces the scenario by observing carbon emissions, compared to the setting when the true scenario is known. We also find that scenario uncertainty can lead to considerable delays in the implementation of green investment projects, emphasizing the importance of timely and precise climate policy information.

1. Introduction

As the global climate is changing, the need for a major decarbonization of the energy system has become evident (Teske, 2019; Bogdanov et al., 2019), while climate change impacts are expected throughout the energy system itself (Stanton et al., 2016; Cronin et al., 2018). While there is little doubt that the low-carbon transition will lead to profound changes in the energy system in the years and decades to come, it is difficult to predict the exact nature of these changes and the pace of the transition. Faced with such uncertainty, the scenario approach has emerged as a means to provide decision-makers with the tools to optimize their actions. Produced with the help of integrated assessment models, transition scenarios are published by international bodies such as the IEA (International Energy Agency), IPCC (Intergovernmental Panel on Climate Change), NGFS (Network for Greening the Financial System), IIASA (International Institute for Applied System Analysis), and used by the economic agents to understand the possible futures they need to prepare for. In particular, the NGFS maintains a database of six transition scenarios, described in detail in Section 3. These scenarios are used by financial institutions to conduct climate stress tests: for example, by comparing the value of a bank's portfolio under orderly and disorderly transition scenario, one may evaluate the risk of disorderly transition.

The scenario approach, however, suffers from a number of drawbacks from the point of view of risk management and asset pricing. In most existing approaches the scenario is assumed to be given and known to the agent, thus the influence of the agent's actions on the scenario, and the imperfect knowledge of the scenario by the agent are not taken into account. Yet, owners of energy assets with a risk of stranding, or of construction permits for green energy projects, make their decisions to sell the asset, or to build the plant, without the perfect knowledge of the scenario to come. Instead, they evaluate the prospects of a given asset/investment based on partial information about the state of the energy transition.

* Corresponding author.
E-mail addresses: mariaflora480@gmail.com (M. Flora), peter.tankov@ensae.fr (P. Tankov).
[1] Present affiliation: Capital Fund Management, 23, Rue de l'Université Paris, 75007 France.

https://doi.org/10.1016/j.eneco.2023.106773
Received 6 April 2022; Received in revised form 14 May 2023; Accepted 27 May 2023
Available online 1 June 2023

In this paper we therefore extend the real options (RO) approach to take into account (i) the transition scenario uncertainty and (ii) the progressive discovery of information about the transition scenario by the investors. Traditional RO theory already acknowledges the value of waiting and postponing the investment decision in favor of flexibility and in view of acquiring more information on the evolution of the underlying stochastic variables affecting the project value. However, the sources of uncertainty in a RO model usually stem from the evolution of asset prices or cost variables specific to the project. We consider an additional layer of uncertainty, that is the uncertainty stemming from the energy transition scenario, potentially affecting the distribution of all stochastic variables. Then, we introduce an active Bayesian learning component to this framework. Namely, the agents continuously update their beliefs regarding the likelihood of being in a certain climate scenario, and evaluate the projects accordingly.

Our approach does not require developing a new integrated assessment model, but instead works with any set of scenarios, provided they contain the required variables to determine the cash flow stream of the energy asset. To incorporate scenario uncertainty, we then add to the scenario database a stochastic model describing progressive information discovery and progressive updates of posterior scenario probabilities in the context of Bayesian learning.

Our paper contributes to different strands of literature. The literature on RO in the context of energy project valuation is vast. Indeed, RO is a prominent approach to evaluate capital investments under uncertainty and irreversibility, and energy projects provide a natural field of application given their relatively high capital costs and the multiple sources of uncertainty relative to commodity prices and future electricity demand and supply. Siddiqui and Fleten (2010) evaluate how a firm may proceed with staged commercialization and deployment of competing alternative energy technologies, and find that the option of investing in such projects increases the value of the firm. Fuss et al. (2012) analyze the impact of uncertainty for deriving the optimal portfolio of energy technologies for a profit-maximizing investor. Boomsma et al. (2012) analyze investment decisions in renewable energy under policy interventions, and find that a feed-in tariff leads to earlier investment. Abadie et al. (2011) employ a binomial lattice model to compute the value of the option to abandon a coal-fired power plant; Laurikka and Koljonen (2006) analyze how the uncertainty related to an emission trading scheme affects the value of an option to invest in a coal power plant; Flora and Vargiolu (2020) use a least-squares Monte Carlo approach to solve the optimization problem of decision making in case of a power producer who is considering switching from a carbon-intensive technology to a renewable one under a carbon price floor; Hach and Spinler (2016) assess the effectiveness of capacity payments in promoting gas-fired generation investments under different degrees of feed-in tariff. Detemple and Kitapbayev (2020) develop a real options model where a firm seeking to build a new power plant has the exclusive choice between two technologies, namely wind and gas.

A related literature is also that of climate-related stranded assets. McGlade and Ekins (2015) employ an IAM and find that a third of oil reserves, half of gas reserves and over 80 per cent of current coal reserves must remain underground to maintain the global temperature rise compared to pre-industrial level below 2 °C. A more recent study (Welsby et al., 2021) finds that the 1.5 °C scenario requires nearly 60 per cent of oil and fossil methane gas, and 90 per cent of coal to remain unextracted. Mercure et al. (2018) estimate, with an integrated global economy-environment simulation model, the discounted global wealth loss from stranded fossil fuel assets. Rozenberg et al. (2020) analyze the impact of alternative policy instruments on costs and dynamics of transition from polluting to clean capital, and study their implications for asset stranding. Van der Ploeg and Rezai (2020) study the determinants of asset stranding in the fossil-fuel industry. Mo et al. (2021) focus on the case of China, and show that carbon pricing increases the risk for newly-built coal power plants to become stranded.

Finally, our paper also relates to the literature on active learning. In this context, closest to our paper is Dalby et al. (2018). They study policy uncertainty in the form of an unexpected downward adjustment of a fixed feed-in tariff (FIT) scheme, with a learning perspective. Their agent expects an adverse transition between two regimes of fixed FIT, and has the option to invest in a green energy project. Our work differs in multiple respects. First, their model pertains to renewable energy policy uncertainty rather than broader transition scenario uncertainty. Second, it is specific to renewable energy (RE) project valuation, while we develop a flexible approach that can be used for several potential applications in decision making analysis. Third, they consider a single policy revision, with two possible regimes: either the change in the FIT payment has not yet occurred (this is the starting point), or it has occurred, and in such a case the value of the option to invest in the green energy project becomes zero. In contrast, our model can include several different scenarios, and climate uncertainty shapes the trajectories of all state variables.

The paper is structured as follows. In Section 2, we present our model of an agent learning the likelihood of a global transition scenario from a climate-related signal, for the purpose of decision-making. In Section 3, we describe an empirical application of our approach, and analyze the sensitivity of our results to a set of parameters. Section 4 concludes.

2. Model and scenario uncertainty with Bayesian learning

2.1. Description of the model

We consider a discrete time model, where the integer-valued variable t denotes time measured in years. In the context of long-term investment/divestment decisions, it seems reasonable to assume that the agent may revise her investment/divestment strategy once a year. A risk-neutral and profit-maximizing economic agent (owner of a power-generating asset or of the potential investment project), facing both revenue risk and scenario uncertainty, has the option to either sell/decommission the asset or to invest into the project at a future date τ. The revenues of the asset prior to closure/of the project after investment are determined by future values of risk factors (fuel prices, electricity price, carbon price) whose evolution is stochastic and whose distribution depends on the realized transition scenario. We assume there are N scenarios corresponding to different climate, economic and policy assumptions. The true scenario is not known to the agent ex ante, however, the agent observes a signal (e.g., global CO2 emissions), which contains noisy information about the scenario, and allows the agent to progressively update her posterior probability of realization for each scenario. For example, if the emissions decrease at a steady rate, the agent will assume that an orderly transition scenario is more likely than a delayed transition scenario.

Under each scenario, consider a number K of stochastic risk factors. We assume that the value $P_{k,t}$ of the risk factor k at time t under the scenario i follows an autoregressive dynamics with scenario-dependent mean $\mu^i_{k,t}$. To write the risk factor dynamics in matrix form, we denote by $\mathbf{P}_t$ the K-dimensional vector of risk factors, by $\boldsymbol{\mu}^i_t$ the vector of scenario-dependent means, by $\boldsymbol{\Phi}$ the $(K \times K)$ matrix of mean reversion rates, and by $\boldsymbol{\sigma}$ the Cholesky decomposition of the instantaneous variance–covariance matrix of the risk factors. Thus, in matrix form we have

$$\mathbf{P}_t = \widetilde{\mathbf{P}}_t + \boldsymbol{\mu}^i_t, \quad \widetilde{\mathbf{P}}_t = \boldsymbol{\Phi}\widetilde{\mathbf{P}}_{t-1} + \boldsymbol{\sigma}\boldsymbol{\varepsilon}_t, \quad t > 0, \quad \widetilde{\mathbf{P}}_0 = 0. \tag{1}$$

under scenario i, where $(\boldsymbol{\varepsilon}_t)$ is a sequence of i.i.d. K-dimensional standard normal vectors.

2.2. Bayesian updates

As mentioned above, the agent does not know the true scenario i, but observes a noisy signal y_t, and infers the likelihood of being in scenario i based on this signal. Ideally, the signal should be a (scenario-dependent) variable that is highly affected by or that has a high correlation with the scenario. Thus, the signal will "reveal" to the agent, with error, the state i. For example, the signal the agent relies on could be the price of carbon in the region where the production asset is located or the agent plans to invest; or the total emissions of greenhouse gases. Let us assume the signal is normally distributed with mean $\mu^i_{y,t}$ and standard deviation σ_y, that is

$$y_t = \mu^i_{y,t} + \sigma_y \eta_t\,, \qquad \text{with} \quad \eta_t \sim N(0,1) \text{ i.i.d.} \tag{2}$$

We assume that, given the scenario, the signal is independent from the risk factors, or, in other words, η_t is independent from ε^k_t for all k. This does not imply that the signal is completely independent from the risk factors, which is not a realistic assumption, but only that their dependence is explained by the scenario. For example, if the signal corresponds to the carbon price and the risk factor is the electricity generation, then in a net zero scenario we expect both of them to rise, but, conditionally on the scenario, the noises of these two processes may be independent.

At every time step, the agent updates her prior knowledge of the state to obtain a posterior probability of each state i. Since our aim is to understand the role of emissions/carbon price as a signal informing economic agents about scenario uncertainty, we assume that the updates are only based on the value of the signal, but not on the values of the risk factors P_t.

The probability π^i_t of being in scenario i at time t based on the signal y_t is

$$\pi^i_t = \mathbb{P}[I = i|\mathcal{F}_t], \quad \mathcal{F}_t = \sigma(y_s, s \le t)\,, \tag{3}$$

where $\{\mathcal{F}_t : t \ge 0\}$ is the filtration generated by the observable process $\{y_t : t \ge 0\}$. In particular, the Bayesian update of π^i_t at each time step t is

$$\begin{aligned}\pi^i_t &= \mathbb{P}[I = i|y_t, \mathcal{F}_{t-1}] = \frac{\mathbb{P}[I = i, y_t \in dy|\mathcal{F}_{t-1}]}{\mathbb{P}[y_t \in dy|\mathcal{F}_{t-1}]} \\ &= \pi^i_{t-1} \frac{\mathbb{P}[y_t \in dy|I = i, \mathcal{F}_{t-1}]}{\mathbb{P}[y_t \in dy|\mathcal{F}_{t-1}]}\,,\end{aligned} \tag{4}$$

where we use the notation $\mathbb{P}[y_t \in dy|\mathcal{F}_{t-1}]$ as a short-hand for the density of y_t given $\mathcal{F}_{t-1}$, and similarly for other notation in the above equation.

The *unnormalized posterior probability* of being in scenario i is then given by

$$\hat\pi^i_t = \hat\pi^i_{t-1} e^{-\frac{\left(y_t - \mu^i_{y,t}\right)^2}{2\sigma_y^2}}, \quad \hat\pi^i_0 = \pi^i_0\,, \tag{5}$$

and the normalized probability is

$$\pi^i_t = \frac{\hat\pi^i_t}{\sum_i \hat\pi^i_t}\,. \tag{6}$$

Provided that the scenarios offer a range of sufficiently diversified trends $\mu^i_{y,t}$ for the signal, the lower the standard deviation of the signal σ_y, the sooner the agent's belief on the likelihood of being in a certain scenario i will converge to either 0 or 1.

In real option theory, the decision making analysis of the agent is similar to the pricing of an American option. To enforce our assumption that the scenario information is extracted solely from the signal, we suppose that the pricing procedure uses only the random part of the risk factors $\widetilde{\mathbf{P}}$, but not the scenario-dependent part. In practice this means that the agent uses a stochastic model for, e.g., the difference between the observed monthly local price and a slowly varying global price index, and uses the scenario information extracted from the signal to project the slowly varying price index.

The value function (value of the asset) at date t is related, through the dynamic programming principle, to the value function at date $t+1$, and computed by backward induction. This approach relies on the specification of a dynamics for the underlying stochastic processes, that is, we need to determine the joint dynamics of the (scenario-independent random parts of the) risk factors, the signal, and the scenario probabilities π^i_t, or, in other words, the rule of updating $\widetilde{\mathbf{P}}_t$, y_t and π^i_t from $\widetilde{\mathbf{P}}_{t-1}$, y_{t-1} and π^i_{t-1}. The rule for updating the probabilities is given by Eqs. (5)–(6) and that for the risk factors is given by Eq. (1). For updating the signal, we compute the conditional law of y_t given $\mathcal{F}_{t-1}$:

$$\mathbb{P}\left[y_t \in B|I = i\right] = \frac{1}{\sqrt{2\pi\sigma_y^2}} \int_B e^{-\frac{\left(z - \mu^i_{y,t}\right)^2}{2\sigma_y^2}}\, dz\,, \tag{7}$$

Thus, conditionally on the information available to the agent, the risk factors and the signal are distributed as a multivariate Gaussian mixture model.

Since the update rule for y_t does not depend on y_{t-1}, the process obtained with this update rule is a Markov process, as shown by the following proposition.

Proposition 1. *Let $(U_t)_{t=0,1,\dots}$ be a sequence of independent random variables with uniform distribution on the interval $[0,1]$, independent from the sequences (ε_t) and (η_t). Define the sequence*

$$\widetilde{\mathbf{P}}_t = \boldsymbol{\sigma}\boldsymbol{\varepsilon}_t + \boldsymbol{\Phi}\widetilde{\mathbf{P}}_{t-1},$$

$$I_t = \min\{i = 1, \dots, N : \sum_{j=1}^{i} \tilde\pi^j_{t-1} \ge U_t\},$$

$$\tilde y_t = \sigma_y \eta_t + \sum_{i=1}^{N} \mathbf{1}_{I_t = i}\, \mu^i_{y,t}$$

$$\tilde\pi^i_t = \frac{\tilde\pi^i_{t-1} e^{-\frac{\left(\tilde y_t - \mu^i_{y,t}\right)^2}{2\sigma_y^2}}}{\sum_{j=1}^N \tilde\pi^j_{t-1} e^{-\frac{\left(\tilde y_t - \mu^j_{y,t}\right)^2}{2\sigma_y^2}}}, \quad i = 1, \dots, N,$$

for $t = 1, 2, \dots$, with initial conditions $\widetilde{\mathbf{P}}_0 = 0$ and $\tilde\pi^i_0 = \pi^i_0$, $i = 1, \dots, N$.

Then the process $(\widetilde{\mathbf{P}}_t, \tilde y_t, \tilde{\boldsymbol{\pi}}_t)$ has the same law as the process $(\widetilde{\mathbf{P}}_t, y_t, \boldsymbol{\pi}_t)$, where y and $\boldsymbol{\pi}$ are defined by

$$y_t = \sigma_y \eta_t + \sum_{i=1}^{N} \mathbf{1}_{I=i}\, \mu^i_{y,t}, \quad \pi^i_t = \mathbb{P}[I = i|\mathcal{F}_t], \quad \mathcal{F}_t = \sigma(y_s, s \le t),$$

where

$$I = \min\{i = 1, \dots, N : \sum_{j=1}^{i} \pi^j_0 \ge U\}$$

and U is an independent random variable with uniform distribution on $[0,1]$.

Proof. Since the risk factors $\widetilde{\mathbf{P}}$ are independent from the scenario, it is sufficient to consider the law of the process $(\tilde y_t, \tilde{\boldsymbol{\pi}}_t)$. Moreover, we have shown by Bayes formula that the conditional probabilities $\boldsymbol{\pi}_t$ satisfy the same update rules (as function of the signal) as the probabilities $\tilde{\boldsymbol{\pi}}$ defined in the proposition. Thus it is sufficient to show that the signal $\tilde y$ defined in the proposition has the same law as the signal y. Further, for any $i = 1, \dots, N$, any $t > 0$, and any bounded measurable f,

$$\begin{aligned}\mathbb{E}[f(\tilde y_t)\tilde\pi^i_t \mid \tilde{\boldsymbol{\pi}}_{t-1}] &= \mathbb{E}\left[\frac{f(\tilde y_t)\tilde\pi^i_{t-1} e^{-\frac{\left(\tilde y_t - \mu^i_{y,t}\right)^2}{2\sigma_y^2}}}{\sum_{j=1}^N \tilde\pi^j_{t-1} e^{-\frac{\left(\tilde y_t - \mu^j_{y,t}\right)^2}{2\sigma_y^2}}} \,\middle|\, \tilde{\boldsymbol{\pi}}_{t-1}\right] \\ &= \mathbb{E}\left[\sum_{k=1}^{N} \frac{f(\sigma_y\eta_t + \mu^k_{y,t})\tilde\pi^k_{t-1}\tilde\pi^i_{t-1} e^{-\frac{\left(\sigma_y\eta_t + \mu^k_{y,t} - \mu^i_{y,t}\right)^2}{2\sigma_y^2}}}{\sum_{j=1}^N \tilde\pi^j_{t-1} e^{-\frac{\left(\sigma_y\eta_t + \mu^k_{y,t} - \mu^j_{y,t}\right)^2}{2\sigma_y^2}}} \,\middle|\, \tilde{\boldsymbol{\pi}}_{t-1}\right]\end{aligned}$$

$$= \frac{1}{\sigma_y\sqrt{2\pi}} \int_{\mathbb{R}} \sum_{k=1}^{N} \frac{f(y+\mu_{y,t}^k)\tilde{\pi}_{t-1}^k \tilde{\pi}_{t-1}^i e^{-\frac{\left(y+\mu_{y,t}^k-\mu_{y,t}^i\right)^2}{2\sigma_y^2}}}{\sum_{j=1}^{N} \tilde{\pi}_{t-1}^j e^{-\frac{\left(y+\mu_{y,t}^k-\mu_{y,t}^j\right)^2}{2\sigma_y^2}}} e^{-\frac{y^2}{2\sigma_y^2}} dy$$

$$= \frac{1}{\sigma_y\sqrt{2\pi}} \int_{\mathbb{R}} \frac{f(y)\tilde{\pi}_{t-1}^i e^{-\frac{\left(y-\mu_{y,t}^i\right)^2}{2\sigma_y^2}}}{\sum_{j=1}^{N} \tilde{\pi}_{t-1}^j e^{-\frac{\left(y-\mu_{y,t}^j\right)^2}{2\sigma_y^2}}} \sum_{k=1}^{N} \tilde{\pi}_{t-1}^k e^{-\frac{(y-\mu_{y,t}^k)^2}{2\sigma_y^2}} dy$$

$$= \frac{\tilde{\pi}_{t-1}^i}{\sigma_y\sqrt{2\pi}} \int_{\mathbb{R}} f(y) e^{-\frac{\left(y-\mu_{y,t}^i\right)^2}{2\sigma_y^2}} dy = \tilde{\pi}_{t-1}^i \mathbb{E}[f(\sigma_y\eta_t + \mu_{y,t}^i)].$$

Fix an integer $T < \infty$ and consider bounded measurable functions $f_1, \dots, f_T$. Then, using repeatedly the previous formula,

$$\begin{aligned}
\mathbb{E}[f_T(\tilde{y}_T)\dots f_1(\tilde{y}_1)] &= \mathbb{E}[\mathbb{E}[f_T(\tilde{y}_T) \mid \tilde{y}_{T-1}\dots\tilde{y}_1] f_{T-1}(\tilde{y}_{T-1})\dots f_1(\tilde{y}_1)] \\
&= \sum_{i=1}^{N} \mathbb{E}[f_T(\sigma_y\eta_T + \mu_{y,T}^i)]\, \mathbb{E}\left[\tilde{\pi}_{T-1}^i f_{T-1}(\tilde{y}_{T-1})\dots f_1(\tilde{y}_1)\right] \\
&= \sum_{i=1}^{N} \mathbb{E}[f_T(\sigma_y\eta_T + \mu_{y,T}^i)]\, \mathbb{E}[f_T(\sigma_y\eta_{T-1}) + \mu_{y,T-1}^i] \\
&\quad \mathbb{E}\left[\tilde{\pi}_{T-2}^i f_{T-2}(\tilde{y}_{T-2})\dots f_1(\tilde{y}_1)\right] \\
&= \dots = \sum_{i=1}^{N} \pi_0^i \prod_{t=1}^{T} \mathbb{E}[f_t(\sigma_y\eta_t + \mu_{y,t}^i)] = \mathbb{E}\left[\prod_{t=1}^{T} f_t(y_t)\right],
\end{aligned}$$

which finishes the proof. □

2.3. Optimal project valuation under scenario uncertainty

Our model is general enough to be applicable in many contexts. In this section, we will focus on two types of investment decisions: (1) an optimal exit problem, where the agent owns a carbon-intensive plant and is considering decommissioning the plant; and (2) an optimal entry problem, where the agent has the option to invest in a green energy project. These problems can be both modeled as an American option pricing problem, and solved numerically by a Least Squares Monte Carlo (LSMC) approach.

In our model, the agent's incentive to delay the investment decision lies not only in the opportunity to wait for future price information, but also in that of learning about the macroeconomic scenario with greater accuracy. The agent has indeed two main sources of uncertainty: the one stemming from the fluctuations of risk factor values $\widetilde{\mathbf{P}}_t$, and the transition scenario uncertainty. This is the main difference with respect to standard real options models, where the value of the underlying only depends on stochastic variables that are commodity prices or other asset prices.

We assume that the agent makes the decision based on the information from the observable risk factor values, and the information about the posterior scenario probabilities deduced from the signal. We thus consider the Markov process $(\mathbf{X}_t := (\widetilde{\mathbf{P}}_t, \boldsymbol{\pi}_t))_{t=0,1,\dots}$ defined in the previous section, and denote by $\mathbb{G} = (\mathcal{G}_t)_{t=0,1,\dots}$ the natural filtration of this process.

1. **Optimal exit**
   The problem of an agent who is considering selling (or decommissioning) a potentially stranded asset can be written as the following optimal stopping problem:

$$\sup_{\tau\in\mathcal{T}} \mathbb{E}\left[\sum_{t=1}^{\tau} \beta^t h(\mathbf{P}_t) - \beta^\tau K(\tau)\right], \tag{8}$$

   where $\mathcal{T}$ is the set of $\mathbb{G}$-stopping times with values in $0, 1, 2, \dots, T$, $h(\mathbf{P}_t)$ is the Profit&Loss function of year t, β is a discount factor that accounts both for the time value of money and for the riskiness of the investment, and K is the cost of decommissioning the plant or, when negative, the price at which the plant is sold. At each point in time until the asset's lifetime T, the agent has to decide whether to continue operating the plant or not.
2. **Optimal entry**
   The problem of an agent who is considering a potential investment before time T_0 in a green energy project with lifetime T can be written as the following optimal stopping problem:

$$\sup_{\tau\in\mathcal{T}} \mathbb{E}\left[\sum_{t=\tau}^{\tau+T} \beta^t h(\mathbf{P}_t) - \beta^\tau K(\tau)\right], \tag{9}$$

   where $\mathcal{T}$ is the set of $\mathbb{G}$-stopping times with values in $0, 1, 2, \dots, T_0$, $h(\mathbf{P}_t)$ is the profit and loss (P&L) function of year t, β is a discount factor, and K is the capital cost needed to undertake the project. At each point in time, the agent has to decide whether to exercise the real option, or to postpone the decision until more precise information about the potential profitability of the project becomes available.

In what follows, to simplify our presentation, we will focus on case (1), that is the optimal exit problem, with the understanding that our setting fully addresses case (2) as well. Introduce the value function

$$\begin{aligned}
V(t, \widetilde{\mathbf{P}}, \boldsymbol{\pi}) &:= \sup_{\tau\in\mathcal{T}_t} \mathbb{E}\left[\sum_{s=t+1}^{\tau} \beta^{s-t} h(\mathbf{P}_s) - \beta^{\tau-t} K(\tau) \,\middle|\, (\widetilde{\mathbf{P}}_t, \boldsymbol{\pi}_t) = (\widetilde{\mathbf{P}}, \boldsymbol{\pi})\right] \\
&= \sup_{\tau\in\mathcal{T}_t} \mathbb{E}\left[\sum_{s=t+1}^{\tau} \beta^{s-t} \sum_{j=1}^{N} \pi_s^j\, h(\widetilde{\mathbf{P}}_s + \boldsymbol{\mu}_s^j) - \beta^{\tau-t} K(\tau) \,\middle|\, (\widetilde{\mathbf{P}}_t, \boldsymbol{\pi}_t) = (\widetilde{\mathbf{P}}, \boldsymbol{\pi})\right],
\end{aligned}$$

where $\mathcal{T}_t$ is the set of $\mathbb{G}$-stopping times with values in $t, \dots, T$. By standard backward induction argument, it can be shown that the value function satisfies the following dynamic programming principle:

$$V(t, \widetilde{\mathbf{P}}, \boldsymbol{\pi}) := \max\left\{-K(t), \beta\mathbb{E}\left[h(\mathbf{P}_{t+1}) + V(t+1, \mathbf{P}_{t+1}, \boldsymbol{\pi}_{t+1}) \,\middle|\, (\widetilde{\mathbf{P}}_t, \boldsymbol{\pi}_t) = (\widetilde{\mathbf{P}}, \boldsymbol{\pi})\right]\right\} \tag{10}$$

$$= \max\{-K(t), CV\left(t, \widetilde{\mathbf{P}}_t, \boldsymbol{\pi}_t\right)\}, \tag{11}$$

where CV is the so called continuation value:

$$CV\left(t, \widetilde{\mathbf{P}}_t, \boldsymbol{\pi}_t\right) = \beta\mathbb{E}\left[h(\mathbf{P}_{t+1}) + V(t+1, \widetilde{\mathbf{P}}_{t+1}, \boldsymbol{\pi}_{t+1}) \,\middle|\, \widetilde{\mathbf{P}}_t, \boldsymbol{\pi}_t\right]. \tag{12}$$

As mentioned, Eq. (10) can be solved numerically by LSMC, that couples backward oriented dynamic programming techniques with forward oriented simulation techniques. The LSMC algorithm works by backward induction, and at each point in time it compares the convenience of immediate exercise with that of delaying the decision. As outlined in Longstaff and Schwartz (2001), the continuation value at each possible exercise point can be estimated from a least squares cross-sectional regression using the simulated paths. The algorithm (see Algorithm 1) then returns both the value of the real option V_t and the optimal exercise time τ. In the algorithm, $\tilde{V}_t$ denotes an auxiliary process whose conditional expectation equals the continuation value.

As the algorithm shows, a crucial part in the LSMC procedure is to use the cross-sectional information in the simulation to estimate the expectation on future cash flows. In all the empirical applications that follow, we employ a quadratic specification to regress the discounted value of the payoff at future dates over the simulated state variables. Specifically, our least-squares specification with which we cross-sectionally regress the continuation values of the different simulated paths j at time t is the following:

$$CV_{t,j} = \alpha_t + \boldsymbol{\vartheta}_t f\left(\boldsymbol{\pi}_{t,j}, \widetilde{\mathbf{P}}_{t,j}\right) + \varepsilon_{t,j}, \tag{13}$$

where $f(\cdot)$ is a second-order polynomial function. A sensitivity analysis with respect to the choice of the basis functions has been performed and shows that the standard quadratic basis provides a good trade-off in terms of improving numerical accuracy and reducing the risk of overfitting in our context.

Algorithm 1: Least Squares Monte Carlo

Simulate N_{sim} realizations of the true scenario I and corresponding trajectories of $X_t = [\pi_t^1, \cdots, \pi_t^N, \widetilde{P}_t^1, \cdots, \widetilde{P}_t^K]$, for $t = 1, \ldots, T$.
For each trajectory, set $\tilde{V}_T = h(\widetilde{\mathbf{P}}_T + \boldsymbol{\mu}_T^I) - K(T)$;
for $t = T-1 : -1 : 1$ **do**
  Perform a polynomial regression of $Y_t = \beta \tilde{V}_{t+1}$ on X_t;
  Use the result to estimate continuation value CV_t on each trajectory
  if $CV_t + K(t) < 0$ **then**
    exercise is optimal on this trajectory;
    $V_t = -K(t)$ and $\tilde{V}_t = h(\widetilde{\mathbf{P}}_t + \boldsymbol{\mu}_t^I) - K(t)$;
  else
    continuation is optimal on this trajectory;
    $V_t = CV_t$ and $\tilde{V}_t = h(\widetilde{\mathbf{P}}_t + \boldsymbol{\mu}_t^I) + CV_t$
  end
end
$V_0 = \frac{\beta}{N_{sim}} \sum \tilde{V}_1$.

3. Empirical application

3.1. Climate scenarios

Integrated assessment models (IAMs) encompassing feedbacks between the global economy, the energy system and the climate system, are the convenient tool to analyze the economic impacts of climate change and climate change mitigation measures. IAMs are used to generate scenarios of evolution of the economy consistent with given climate objectives, based on a set of assumptions.

In this section, we illustrate how our method can be applied to model transition scenario uncertainty. We employ scenario data from an IAM in the NGFS scenario database,[2] namely REMIND-MAGPIE 3.0–4.4. This model is a global multi-regional general equilibrium model with a rather detailed representation of the energy system, belonging to the class of intertemporal optimization models with perfect foresight.

The NGFS scenario database includes 6 alternative scenarios produced with REMIND 3.0 model:

- **Current Policies:** existing climate policies remain in place, and there is no strengthening of ambition level of these policies;
- **Nationally Determined Contributions (NDCs):** currently pledged unconditional NDCs are implemented fully, and respective targets on energy and emissions in 2025 and 2030 are reached in all countries;
- **Delayed Transition (Disorderly):** there is a "fossil recovery" from 2020 to 2030; thus this scenario follows the trajectory of the Current Policies scenario until 2030. Only thereafter countries with a clear commitment to a specific net-zero policy target at the end of 2020 are assumed to meet the target, representing regional fragmentation. Regionally fragmented carbon prices converge to a global price near 2070 to keep the 67-percentile of warming below 2 °C in 2100, which also allows for temporary overshoot;
- **Below 2 °C:** this scenario assumes that optimal carbon prices in line with the long-term targets are implemented immediately after 2020 and keeps the 67-percentile of warming below 2 °C throughout the 21st century;
- **Divergent Net Zero (Disorderly):** optimal carbon prices in line with the long-term targets are implemented immediately after 2020 to bring the median temperature below 1.5 °C in 2100, after a limited temporary overshoot. Policy pressure and mitigation efforts are unevenly distributed across sectors;
- **Net Zero 2050:** global CO_2 emissions are at net-zero in 2050. Furthermore, countries with a clear commitment to a specific net-zero policy target at the end of 2020 are assumed to meet this target.

From top to bottom, the scenarios display a range of levels of stringency of the climate policy that underlies scenario assumptions. Thus, each scenario entails different paths for the macroeconomic variables in the model, and overall they provide a comprehensive overview of the possible climate states.

[2] Release 3.4, available at https://data.ene.iiasa.ac.at/ngfs/.

Table 1
Variables used in the plant evaluation.

Variables	Name	Units
Capital costs	C_C	USD2010/kW
O&M costs, fixed	C_F	USD2010/MW/year
O&M costs, variable	C_V	USD2010/MWh
Fuel price	P_F	USD2010/MWh
Conversion efficiency	R_C	per cent
Carbon price	P_C	USD2010/t CO2
Electricity price	P_E	USD2010/MWh
Net electricity production	Q	GWh
Total installed capacity	T	GW
Emission rate	R_E	t CO2/MWh
Plant rated power	W	MW

3.2. Optimal exit from a carbon-intensive power plant

As a first empirical application, we consider an agent who owns a pulverized coal power plant with combined cycle, without Carbon Capture and Storage (CCS) technology, and wants to know when it is economically optimal to decommission (or sell) the plant. We assume the cost of decommissioning the plant corresponds to a fraction k of the capital cost of building a new coal power plant, C_C^c. When k is negative, the agent is selling the plant at price $k\,C_C^c$. In the results showcased in Section 3.2.1, unless specified otherwise, we assume $k = 0$, *i.e.* there are no decommissioning costs. A sensitivity analysis for this parameter is shown is Section 3.2.2. The plant is a price taker, and supplies every year a quantity of electricity which depends on the plant's utilization rate (a variable available in each scenario) but not on energy prices. We assume it has a nominal capacity $W = 1000\,\text{MW}$ and it is located in Germany. We further suppose that the plant has a residual lifetime of 30 years, thus, assuming $t_0 = 2020$, we restrict our investment valuation framework to years 2020–2050 of the scenario dataset. Finally, we assume a risk-adjusted discount factor $\beta = e^{-r\Delta t}$, with $r = 1\%$ unless specified otherwise. Because it is not equipped with a CCS filter, the plant has to buy some emission allowances in every period, to comply with an emission trading scheme (ETS). Moreover, in every period, it incurs some operation and maintenance (O&M) costs, both fixed (C_F^c) and proportional to the production output (C_V^c). The production output of the plant depends on the plant utilization rate R_U^c, which equals the ratio of the yearly net electricity production Q^c to the total installed capacity T^c for this specific technology in the selected region. The P&L function of year t of the coal plant, with the appropriate conversion factors, is thus equal to

$$h_t^c = W \cdot R_{U\,t}^c \cdot 365.25 \cdot 24 \left(P_{E\,t} - \frac{P_{F\,t}}{R_C^c} - R_E^c P_{C\,t} - C_V^c \right) - W \cdot C_F^c, \quad (14)$$

where

$$R_{U\,t}^c = \text{Utilization rate} = \frac{Q_t^c}{T_t^c \cdot 365.25 \cdot 24}. \quad (15)$$

The variables used and their corresponding unit of measure are listed in Table 1 (we omit the superscript c, indicating the coal technology, to avoid clutter).

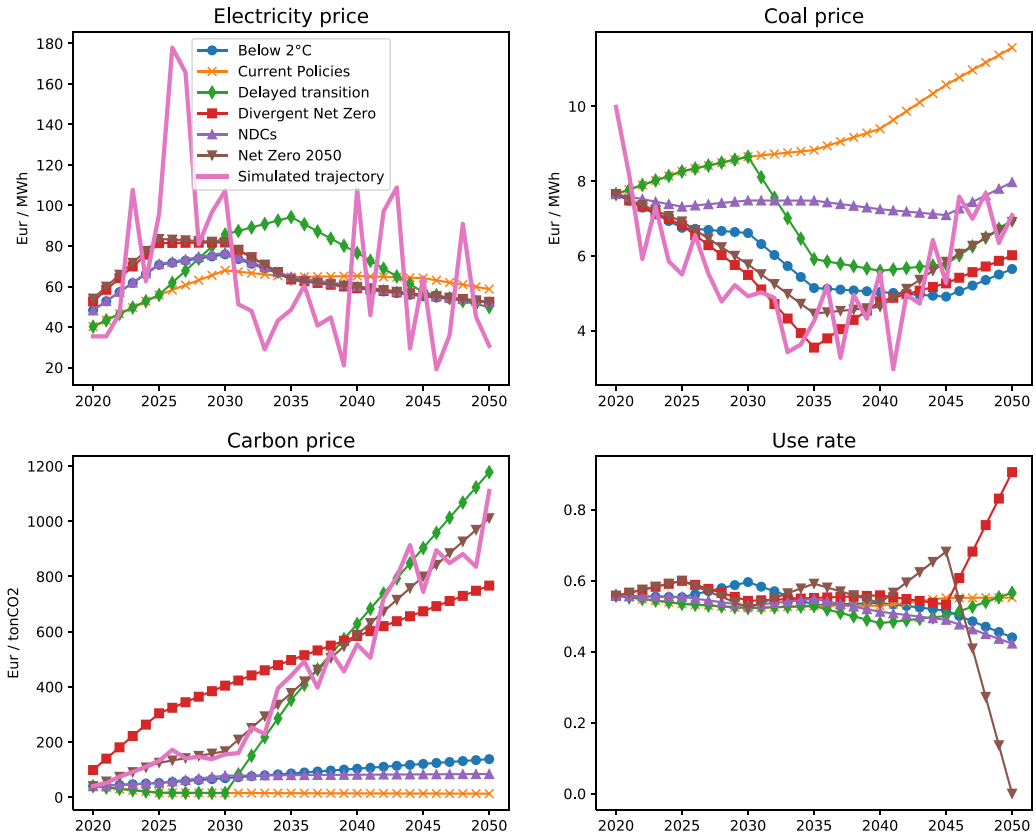

Fig. 1. Evolution of the mean value of the three risk factors and of the coal utilization rate in the different scenarios produced with the REMIND 3.0 IAM, together with a sample simulation of the three risk factors.

Some of the variables in (14) are more likely to have a high variability, and thus we model them as stochastic, according to (1). Such risk factors, in this example application, are

$$\mathbf{P} = \begin{pmatrix} P_E \\ P_F \\ P_C \end{pmatrix}.$$

As mentioned, their mean values $\mu^i_{\cdot,t}$ depend on the scenario i of the chosen scenario dataset, and are given by the corresponding ith scenario path for that variable. Fig. 1 plots the evolution of the mean value $\mu^i_{k,t}$ of each risk factor together with a sample simulation of the three risk factors. All other variables in Eq. (14) except for the risk factors are modeled as deterministic, and their time-dependent values are extracted from the scenario database, when available. Moreover, when possible (for coal, carbon and electricity price), the variables are taken from the downscaled NGFS data for the specific region, otherwise (for capital costs and utilization rate) the variables for the EU-28 region of the original REMIND 3.0 model are used. For example, the right bottom graph in Fig. 1 shows the evolution of the coal utilization rate in the six scenarios; it is clear that the variability of this quantity is much lower than that of the risk factors. In addition, we assume constant fixed costs C^c_F at 58,000 EUR/MW/year (see ACIL, 2014), variable costs C^c_V at 2.6 EUR/MWh, conversion efficiency R^c_C of 48% and emission rate R^c_E of 0.71 tonCO2 per MWh of electricity generated (see Metz et al., 2007, Sec. 4.4.3.1).

The parameters $\boldsymbol{\Phi}$ and $\boldsymbol{\sigma}$ in (1) are estimated from historical data. Specifically, we use front-month futures data at the monthly frequency from January 2015 to October 2021 of ICE Rotterdam Coal and of ICE EUA (carbon allowances traded in the EU ETS). For electricity, we employ the average hourly price in the day-ahead market for electricity in Germany traded in the EEX, at the monthly frequency. All data were retrieved using the Macrobond database. Because seasonality is a peculiar stylized fact of electricity prices, we first de-seasonalize our monthly log-price electricity sample with a sinusoidal function accounting for half-yearly and annual seasonality. As for carbon and coal log-prices, we de-trend them by subtracting the annual mean level and a linear trend (see Fig. 2). We then estimate a multivariate autoregressive model by maximum likelihood using (de-trended) log-prices. Table 2 shows the resulting estimates for the mean-reversion rates and for the volatility parameters. In the empirical application that follows, we will only employ estimates that are significant at the 95% level, i.e. all entries in the matrix Σ, and all diagonal entries in $\boldsymbol{\Phi}$.

To update her beliefs about the transition scenario, the agent needs to choose which signal to rely on. In this illustration, we assume that

Table 2
Monthly parameter estimates of (1) obtained by estimating a multivariate autoregressive model on de-trended prices of electricity, coal, and carbon.

		E	F	C
Φ	E	0.552*** (0.095)	0.023 (0.031)	0.019 (0.028)
	F	−0.232 (0.261)	0.779*** (0.085)	−0.093 (0.077)
	C	0.173 (0.354)	0.119 (0.116)	0.382*** (0.104)
Σ	E	0.174*** (0.027)	0.015** (0.007)	0.007*** (0.003)
	F	0.015** (0.007)	0.018*** (0.006)	0.004** (0.002)
	C	0.007*** (0.003)	0.004** (0.002)	0.015*** (0.002)

Standard errors are in parenthesis. * = $p < 0.1$, ** = $p < 0.05$, *** = $p < 0.01$.

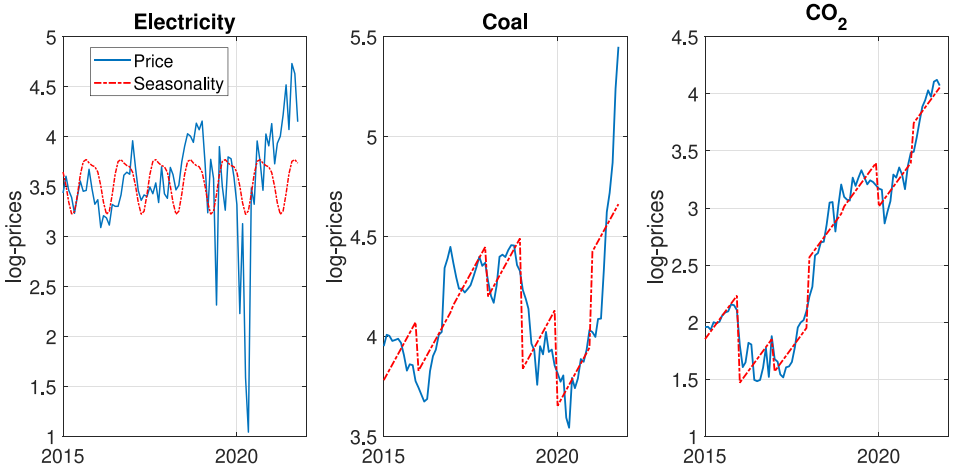

Fig. 2. From left to right, EEX day-ahead electricity log-prices in Germany, ICE Rotterdam front-month futures log-prices, ICE EUA front-month futures log-prices (blue lines), and their relative de-trending (red dotted lines). (For interpretation of the references to color in this figure legend, the reader is referred to the web version of this article.)

the agent chooses the greenhouse gases (GHG) emission level from energy production in the region where the plant is located (Germany). To estimate the volatility of such a signal y, we use a yearly time series from the Macrobond data set, spanning almost 50 years (from 1970 to 2018), and we fit a Gaussian model. The estimated annual signal volatility parameter is $\hat{\sigma}_y = 108.75$ million tons of CO_2 equivalent. We then employ this value to simulate the signal as in Proposition 1. On the bottom graph, Fig. 3 shows a simulated sample path for the signal y_t (solid line), when using the scenarios from the REMIND 3.0 model. The REMIND 3.0 values of the mean GHG emissions path in each scenario are represented by the dashed lines. On the top graph, the figure shows the corresponding evolution of the relative conditional probabilities π_t^i, for $i \in \{1, \dots, 6\}$, computed as in Eq. (6) (where the marks indicating the scenario are the same in both graphs). In this case, the conditional probability of the scenario "Below 2° C" approaches one, while the others converge to zero;

All simulation examples below use $N_{sim} = 200,000$ simulated trajectories.

3.2.1. Numerical results

First, before moving on to analyze the impact of scenario uncertainty revealed by the signal, we compute the value of the project in each individual scenario (assumed known by the agent), the expected optimal exit date for each individual scenario, and the expected value of the project if it operates for the entire lifetime of 30 years with no possibility of exit. This information is shown in Table 3. We see that there are three classes of scenarios: in the least constrained scenario (current policies) it is optimal to operate the plant until the end of its lifetime; in the three intermediate scenarios (below 2° C, delayed transition and NDCs), it is optimal to stop after 10–11 years, and finally in the most constrained scenarios (divergent net zero and net zero 2050) immediate exit is optimal. Stopping at the optimal time leads to a positive value for the plant in all but the most constrained scenarios (where the plant has a small negative value because stopping is only possible after one year of operation). On the other hand, operating the plant until the end of its lifetime has a negative net present value in all but one scenario and entails a particularly massive loss in three of them. Determining the optimal exit time precisely is thus very important in this context.

We now proceed to analyze the impact of the scenario uncertainty. Different scenario datasets may differ not only in the nature of the base assumptions underlying the scenario specifications, but also in the number of scenarios itself. The NGFS REMIND 3.0 dataset offers 6 different scenarios, as discussed in Section 3.1. The ones that matter the most in the context of this empirical application are the ones

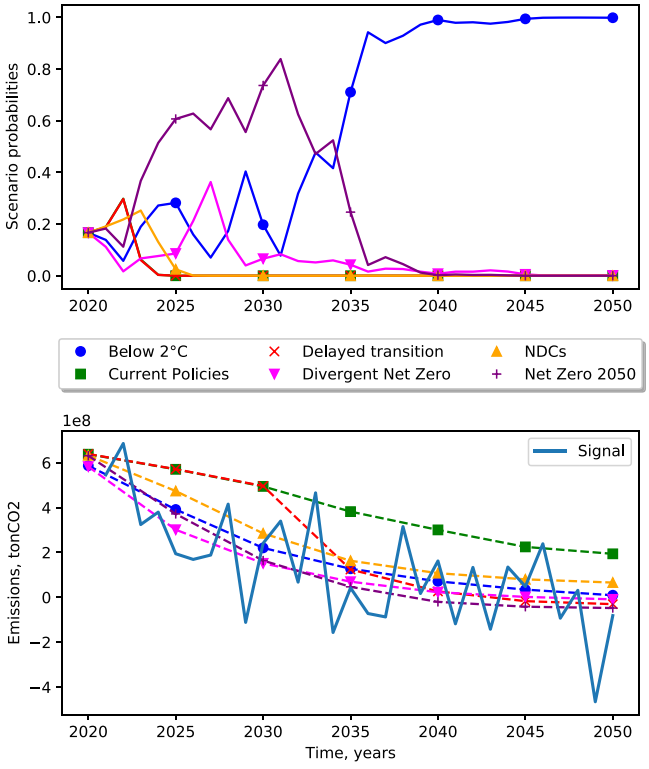

Fig. 3. Bottom graph: a simulated path for the signal y_t (solid line), together with the GHG emission trend evolution in each of the six scenarios according to REMIND 3.0 data. Top graph: conditional probabilities π_t^i, for $i \in \{1, \dots, 6\}$ estimated from the observations of the signal. The marks are the same in both graphs and indicate the specific scenario. For illustration purposes, here the signal volatility was taken equal to 2 times the estimated value.

related to the emissions trajectory, since the signal the agent relies on is closely related to this variable. The span of the paths of this variable in different scenarios represents in a sense the extent to which the agent can decode the state of the system and form a belief about possible implications. It is thus important that the agent has a number of sufficiently diversified scenarios available. To see this, first, let us consider the case when an agent has only two available emission scenarios, and let us suppose that the two are very far apart in their range of values for the emissions variable. If scenarios have a range of values much wider than the variability in the signal, the signal,

Table 3
Project values with and without possibility of exit, and optimal exit times in the absence of scenario uncertainty.

Scenario	Below 2 °C	Current Policies	Delayed transition	Divergent Net Zero	NDCs	Net Zero 2050
Project value, MEur	426	2777	992	−315	254	−15
Project value, MEur, no exit	−1942	2777	−28319	−40080	−1191	−26937
Optimal exit time	11.02	30	11	1	9.21	1

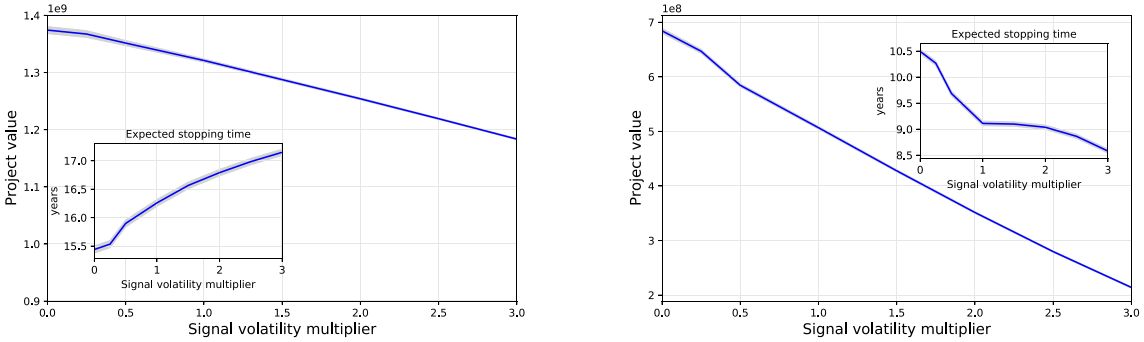

Fig. 4. Optimal exit problem. Sensitivity of the project value (in EUR) to the volatility of the signal, σ_y. In the figure, σ_y varies in a range $[0; 3\,\hat{\sigma}_y]$. In the left panel, only scenarios "Current Policies" and "Net Zero 2050" from the REMIND 3.0 are included in the model. In the right panel, all scenarios are included. The shaded gray area represents the 95% confidence interval (sometimes invisible because it is too narrow). The inset plot shows the sensitivity of the average waiting time before divestment τ to the volatility of the signal σ_y, with a 95% confidence interval.

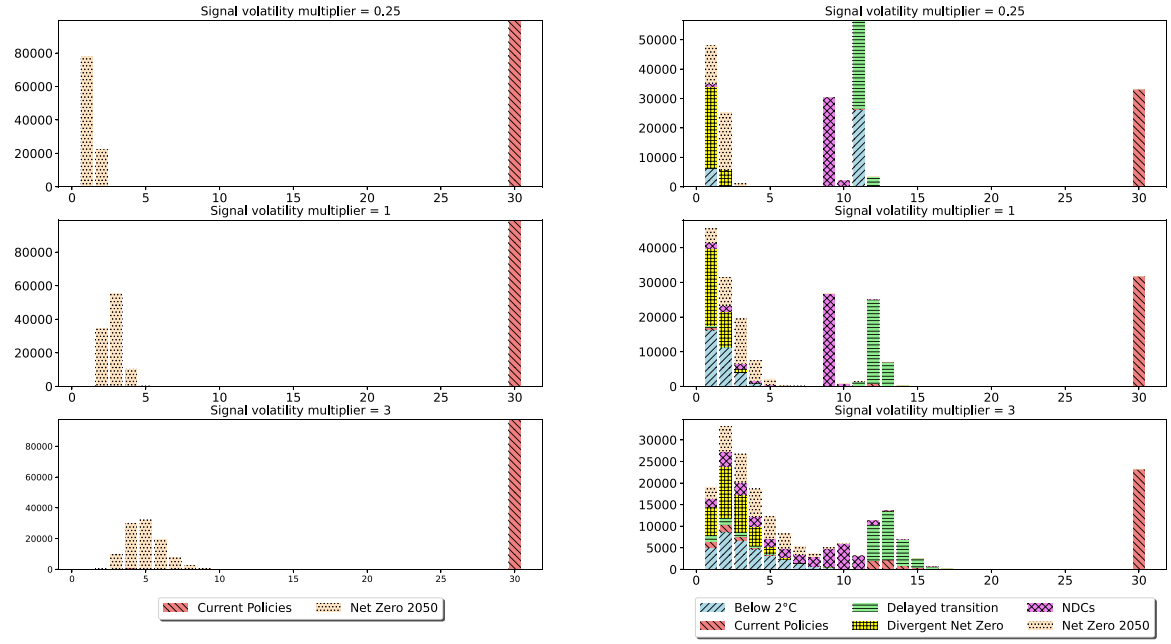

Fig. 5. Optimal divestment timing under scenario uncertainty: distribution of the optimal exit times according to the true scenario. Top row: $\sigma_y = 0.25\,\hat{\sigma}_y$, middle row: $\sigma_y = \hat{\sigma}_y$, bottom row: $\sigma_y = 3\,\hat{\sigma}_y$. In the left graphs, only scenarios "Current Policies" and "Net Zero 2050" are included. In the right graphs, all scenarios are included.

albeit noisy, will likely immediately identify the state of the system, and climate uncertainty would immediately resolve. In this case, the learning process of the agent would end soon, and it would thus not affect much the value of the real option.

Our results confirm this intuition. Indeed, Fig. 4, left graph, shows the sensitivity in the results of our model to the value of the volatility of the signal in the case of two divergent scenarios, "Current Policies" and "Net Zero 2050". We let the signal volatility vary in a range $[0; 3\,\hat{\sigma}_y]$. As Fig. 3 shows, these two scenarios entail very different trajectories for the GHG emissions. When the signal volatility is in a range of 0 to 0.5 times the estimated $\hat{\sigma}_y$, which is not sufficient to cover the range of values spanned by the two scenarios, the value of the project and the optimal exercise time change at a slow pace, and it is only for higher values of signal volatility that the project value starts to decline quickly due to information loss. We remark also that the expected optimal exit time increases as function of signal volatility. To understand this effect, one may examine Fig. 5, left graphs, which show the distribution of optimal exit times for each of the two scenarios. We see that when the signal volatility is high (lower panel), the "Current policies" scenario is stable, meaning that when this scenario is the true one, the agent is

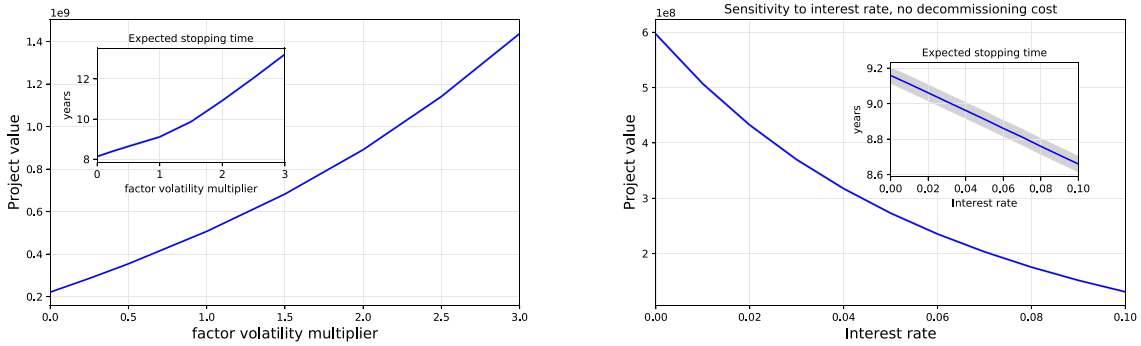

Fig. 6. Optimal exit problem. Sensitivity of the project value (in EUR) to the risk factors volatility, Σ (left panel) and to the discount rate r (right panel). In the left panel, Σ varies in a range $[\frac{1}{4}; 5\,\hat{\Sigma}]$, and the project value is computed with a risk-adjusted discount rate $r = 1\%$. All scenarios from REMIND 3.0 dataset are included. The shaded gray area represents the 95% confidence interval. The inset plot shows the sensitivity of the average waiting time before divestment τ, with a 95% confidence interval.

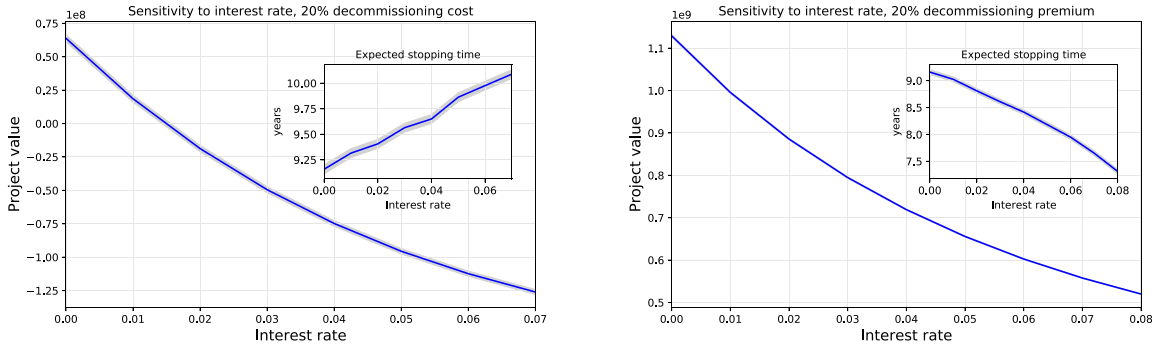

Fig. 7. Sensitivity of the project value (in EUR) to the discount rate. Left decommissioning cost equal to 20% of the capital costs. Right: decommissioning premium (selling revenue) equal to 20% of the capital costs.

Table 4
Value of the investment opportunity and optimal exit times in the absence of scenario uncertainty.

Scenario	Below 2 °C	Current Policies	Delayed transition	Divergent Net Zero	NDCs	Net Zero 2050
Project value, MEur	747	0	1810	1454	177	1390
Optimal investment time	3	∞	6.02	2	2.99	1.37

unlikely to make wrong decision and stop early. On the other hand, the "Net Zero 2050" scenario is unstable: when this scenarios the true one and the signal is very noisy, the agent may spend a long time learning the true scenario before finally deciding to stop.

Fig. 4, right graph, shows the results of our model when all six available scenarios from REMIND 3.0 are included. In this case, scenarios span a wide range of possible trajectories for the GHG emissions, so that the learning process of the agent is more important in her decision making. Indeed, now the value of the real option declines quickly as the signal volatility increases and the information available to the agent becomes more noisy. To understand the decreasing profile of the optimal exercise time, once again we examine the distribution of stopping times in each scenario in Fig. 5, right graphs. We see that while the "Current policies" scenario remains quite stable, the intermediate scenarios such as "NDCs" and "Below 2° C" are less so: when one of this scenarios is the true one, and the signal is very noisy, the agent may mistakingly think that the true scenario is one of the two most constrained ones ("Net Zero 2050" or "Divergent Net Zero") and stop early. Indeed, by looking at Fig. 3 it is clear that these four scenarios are hard to distinguish in the beginning. We then conclude that while the price of the real option always decreases with increasing scenario uncertainty, the expected waiting time until exit may both increase and decrease, depending on the nature of the underlying scenarios.

In applications of our model, we recommend using a sufficiently large number of sufficiently diverging scenarios, so as to describe the range of possible futures in a realistic way.

3.2.2. *Sensitivity analysis*

A crucial parameter in our model is the discount rate reflecting the riskiness of the investment project. Thus, we perform a sensitivity analysis to assess the extent to which our results are affected by the choice of this parameter. Economic intuition commands that lower discount factors β, and thus higher discount rates r, will lead to underweighting future cash flows, and thus to lower values of the project. Indeed, the right panel of Fig. 6 shows that the project value declines as r increases in the range $[1\%; 8\%]$. The inset panel in the figure also shows a mild decrease in the optimal stopping time. This figure also shows the sensitivity to another set of parameters, that is the estimated risk-factors' variance–covariance matrix Σ (left panel). Here, we multiply the estimated variance–covariance matrix by a factor that varies in a range $[\frac{1}{4}; 5]$. When risk factors are more volatile, the flexibility given by owning the option is more valuable, and the RO value is higher. The uncertainty related to the risk factors leads to postponing the decision, and thus to a longer optimal waiting time.

To better understand the impact of the interest rate on the optimal stopping time and at the same time study the impact of decommissioning costs or selling revenues on the real option value, we plot in Fig. 7

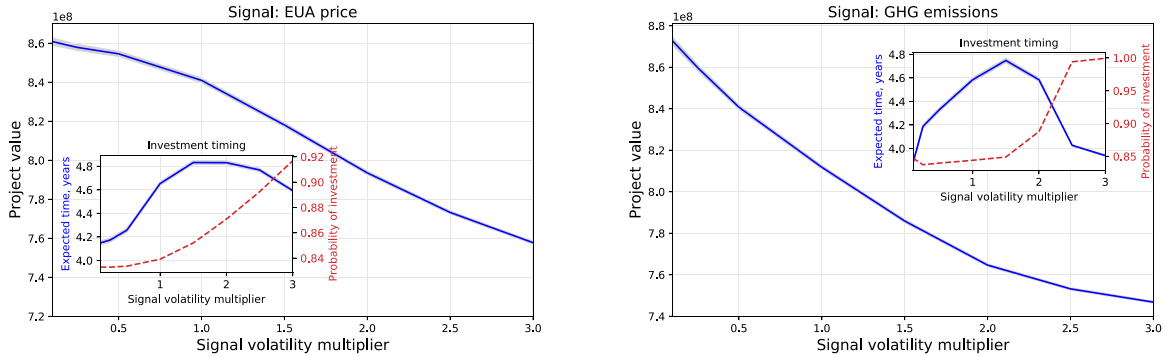

Fig. 8. Optimal entry problem. Sensitivity of the project value (in EUR) to the volatility of the signal, σ_y. In the figure, σ_y varies in a range $[0.1, 3\,\hat{\sigma}_y]$. In the left graph, the EUA emission allowance price is used as the signal. In the right graph, the carbon emissions from energy production in Germany are used. The inset plot shows the sensitivity of the average optimal waiting time before investment, conditional on the investment taking place (solid line, left scale), and the sensitivity of the probability of the investment (dotted line, right scale), to the volatility of the signal σ_y.

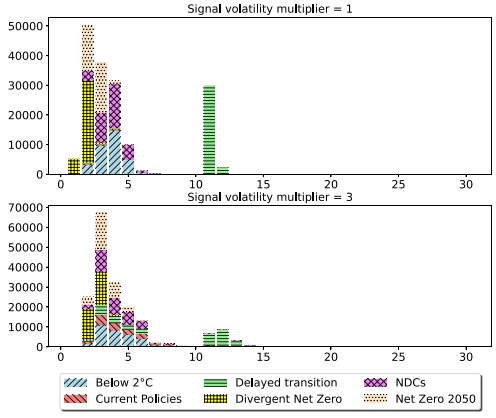

Fig. 9. Optimal investement timing under scenario uncertainty: distribution of the optimal investment times according to the true scenario. Top: $\sigma_y = \hat{\sigma}_y$, bottom: $\sigma_y = 3\hat{\sigma}_y$. EUA emission allowance price is used as the signal.

the sensitivity of the project value and optimal stopping time to the interest rate in the presence of such costs and revenues. In the presence of a positive decommissioning cost (negative cash flow, left graph), the optimal stopping time is increasing as function of the interest rate: for higher rates the agent prefers to wait longer before paying the decommissioning cost, so that its impact is reduced by discounting. In the presence of a decommissioning premium (right graph), the stopping time is decreasing as function of the interest rate: for higher rates the agent prefers to stop earlier to benefit from the decommissioning premium before its value is reduced by discounting. The case when there are no decommissioning costs and no premium is an intermediate one, when there are both positive and negative cash flows and none of them clearly dominates the other. For this reason, in Fig. 6, right graph, we observe only mild dependence of the optimal exit time on the discount rate.

This analysis shows how, by providing a decommissioning premium to carbon-intensive power plants, or by helping them reduce the decommissioning costs, the regulator may accelerate the low-carbon transition of the electrical energy industry.

3.3. Optimal entry in a green investment project

As a second empirical application, we consider an agent who has the option to invest in a combined cycle coal-fired power plant with Carbon Capture and Storage (CCS) technology, and wants to know when it is economically optimal to exercise the RO. The plant is again a price taker, and will supply electricity inelastically. We assume it has a nominal capacity $W = 1000$ MW and is located in Germany. We further assume the plant will have a lifespan of $T = 50$ years, and we assume $t_0 = 2020$. We set the maturity of the RO to be $T_0 = 2050$. Finally, we assume a risk-adjusted discount factor $\beta = e^{-r\Delta t}$, with a reference discount rate of $r = 3\%$. The value of interest rate is higher than in the previous example since the project value is very sensitive to the interest rate in the present case, and the low value of 1% leads to unrealistic results. Sensitivity to the interest rate parameter is analyzed in the following paragraph. The problem the agent needs to solve is now that of Eq. (9). Exercising the option entails a stream of revenues and costs starting from the exercise time τ throughout the plant lifetime, T. The strike price of the RO corresponds to the capital cost of building a new power plant, C_C^{gc} (with gc standing for green coal). Namely, the payoff of the RO at time τ is

$$\max\left(0\,;\mathbb{E}\left[\sum_{t=\tau}^{\tau+T}\beta^{t-\tau}h^{gc}(\mathbf{P}_t)\right]-C_C^{gc}(\tau)\right).$$

If the agent exercises the option, and thus builds the power plant, in every period t she will incur some output-dependent operation and maintenance (O&M) costs, both fixed (C_F^{gc}) and proportional to the production output (C_V^{gc}). The production output of the plant depends on the plant's utilization rate R_U^{gc}. The P&L function of year t of the plant, with the proper conversion factors, is thus equal to

$$h_t^{gc} = W \cdot R_{U\,t}^{gc} \cdot 365.25 \cdot 24\left(P_{E\,t} - \frac{P_{F\,t}}{R_C^{gc}} - C_V^{gc}\right) - W \cdot C_F^{gc}\,. \tag{16}$$

We refer the reader to Table 1 for the explanation of the remaining variables in Eq. (16), as well as for the variables' units of measure.

The risk factors in this example application, that we model according to (1), are now two:

$$\mathbf{P} = \begin{pmatrix} P_E \\ P_F \end{pmatrix}.$$

Indeed, since the plant is a green investment, it is not required to comply with an ETS, and thus it does not have any carbon-related costs.[3] As before, the risk factors' mean values $\mu_{\cdot,t}^i$ depend on the scenario i of the chosen scenario dataset, and are given by the corresponding ith scenario path for that variable. The random parts of the risk factors are modeled as in the previous example, and we use the same estimated parameter values.

In this case, the agent chooses to use as a signal the price of the EUA. To estimate the volatility of such a signal y, we employ the EEX EUA front-month futures detrended monthly log-prices and we fit a Gaussian

[3] In reality, modern CCS technology can only capture about 90% of the emissions, but we neglect the residual emissions in our stylized model since our aim is to illustrate the case of a green investment.

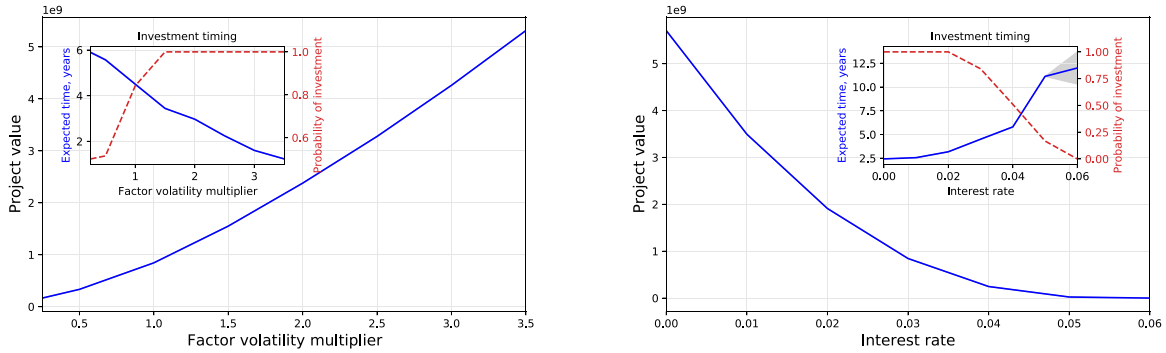

Fig. 10. Optimal entry problem. Sensitivity of the project value (in EUR) to the risk factors volatility, Σ (left panel) and to the discount rate r (right panel). In the left panel, Σ varies in a range $[\frac{1}{4}\hat{\Sigma}; 5\hat{\Sigma}]$. The inset plot shows the sensitivity of the average optimal waiting time before investment, conditional on the investment taking place (solid line, left scale), and the sensitivity of the probability of the investment (dotted line, right scale). The confidence interval is large for high interest rate because investment only happens on a small number of trajectories.

model. The estimated monthly signal volatility parameter is $\hat{\sigma}_y = 0.317$. We then employ this value to simulate the signal as in Eq. (2). For comparison, we also plot the impact of the scenario uncertainty using GHG emissions as the signal (the same one as in the first example).

All variables in Eq. (16) except for the risk factors are modeled as deterministic, and they follow a trend depending on the availability of scenario trajectories for each one of them. In this case, the REMIND 3.0 model includes scenario paths for the risk factors and for the capital cost C_C^b. However, the total installed capacity of coal-fired power plants and the electricity production from coal is not available after 2050. For this reason, we use a fixed utilization rate $R_U^{gc} = 85\%$ (International Energy Agency, 2020). Following the same source, the O&M costs of a coal-fired power plant with CCS are summarized as variable costs of 19.34 USD/MWh. The conversion efficiency is assumed to be $R_C = 48\%$ as in the previous example.

3.3.1. Numerical results

First, before analyzing the impact of scenario uncertainty, we compute the value of the project and the optimal investment time in each individual scenario, assumed known by the agent. This information is shown in Table 4. In the "Current policies" scenario, due to relatively high coal prices and low electricity prices, it is never optimal to invest in a CCS coal power plant, and the project value is zero. In other scenarios, investment happens relatively quickly, except for the delayed transition scenario, where it is optimal to wait for some time to allow the coal prices to go down.

We now proceed to analyze the impact of scenario uncertainty. Fig. 8 shows the sensitivity of both the RO value and the optimal exercise time to the value of the volatility of the signal for the entry problem, when all six available scenarios from REMIND 3.0 are included. We let the signal volatility vary in a range between 10% and 300% of the estimated value. The left graph uses the EUA emission allowance price as the signal, and the right graph uses the GHG emissions from energy production in Germany. The inset plots show the expected stopping time at which the investment takes place, and the probability of the investment. In this problem, on some trajectories it is never optimal to invest, and these trajectories are not taking into account in the computation of the expected stopping time.

Both signals have similar impact on the project value and the investment strategy. In particular, the optimal investment time is first increasing, as the agent needs to wait longer to acquire information, and then starts to decrease, as the signal becomes too noisy and its information value drops. The probability of investment increases with signal volatility, as it becomes more difficult for the agent to precisely detect the only scenario in which investment is not optimal (current policies). Finally, the GHG emissions appear to have a higher information value for the agent than the EUA emission allowance price, as the project value drops faster in the latter case.

To better understand the optimal investment timing in this case, we plot in Fig. 9 the distribution of optimal investment times according to true scenario, when EUA emission allowance price is used as the signal. For higher volatility values, investment happens earlier in the delayed transition scenario, and in some cases even in the current policies scenario (where it is not optimal to invest under full information), because the low information content of the signal does not allow the agent to distinguish these scenarios from the ones where early investment is optimal.

Fig. 10 shows the sensitivity of the RO value, of the average optimal investment time conditional on the investment taking place, and of the investment probability, to the volatility of the risk factors Σ (left panel) and the discount rate r (right panel). We let r vary in a range $[1\%; 6\%]$, and we multiply the estimated variance–covariance matrix by a factor that varies in a range $[\frac{1}{4}; 5]$. As in the optimal exit problem, the RO value is increasing in the volatility of the risk factors and decreasing in the discount rate. However, here, the average optimal exercise time is decreasing in the volatility of the risk factors. Thus, the higher the variability relative of the future cash flows, the earlier it is convenient to invest in the green energy project. The probability of investment is sharply decreasing as function of the interest rate: the construction of a green coal power plant requires a large up-front payment, and for high interest rates, none of the NGFS scenarios promise sufficiently high cash flows to compensate this after discounting.

4. Conclusions

In this paper, we present a new strategy for evaluating investment projects, by combining standard real options techniques with a macroeconomic approach for climate transition analysis. In our model, the agent observes a noisy climate-related signal, and forms a belief relative to the likelihood of the possible current macroeconomic climate scenarios. The agent then bases her entry or exit decisions on the posterior probability of being in a certain macroeconomic scenario. The agent's learning about the level of climate risk, via Bayesian updating, then plays an active role in the decision making process.

We showcase the potential of our strategy using public available scenario data from the NGFS scenario database, which are representative of a range of several different environmental transition pathways. Each of them is associated to a certain level of climate policy stringency, from low (existing climate policies remain in place, with no further effort to mitigate climate change), to high (there is a clear commitment to a specific net-zero policy target that results in CO_2 emissions to be at net-zero in 2050).

These scenarios are employed to analyze the value of real options in two energy-related examples: the divestment decision from a coal-fired power plant without Carbon Capture and Storage (CCS) technology and the potential investment into a green coal-fired power plant with CCS.

In both cases, we find that the real option value is very sensitive to scenario uncertainty: the value of the coal-fired power plant is reduced by 25% and that of the green coal investment project is reduced by 7% when the agent deduces the scenario by observing carbon emissions, compared to the setting when the true scenario is known. We also find that scenario uncertainty can lead to considerable delays in the implementation of green investment projects. These results underscore the importance of reliable and detailed climate scenarios and indicate that taking into account scenario uncertainty and its progressive resolution is essential for precise valuation of energy projects and for determining the optimal investment timing.

The main limitation of our study is that it is based on a stylized model of power plant operation and uses low-granularity scenario data from the NGFS database: some variables are only available for the entire EU-28 region and the time step is generally 5 years before 2050 and 10 years after this date. Features like higher time granularity and increased geographical diversity would add precision to our results. Finally, for the purpose of energy project valuation, it would be important to have an IAM that includes energy producer-specific variables, such as the wholesale price of electricity at the primary level, rather than at the secondary one (which also includes dispatching costs).

CRediT authorship contribution statement

Maria Flora: Conceptualization, Methodology, Data curation, Original software implementation, Writing – original draft. **Peter Tankov:** Conceptualization, Methodology, validation, Final software implementation, Writing – original draft,Writing – review & editing, Supervision, project administration, funding acquisition.

Declaration of competing interest

The authors declare that they have no known competing financial interests or personal relationships that could have appeared to influence the work reported in this paper.

Data availability

This paper uses data from Macrobond (www.macrobond.com) available through paid subscription, for parameter estimation, and publicly available data from the NGFS scenario explorer (https://data.ene.iiasa.ac.at/ngfs) for scenario projections. The code for producing the figures and the estimated parameter values can be downloaded from https://github.com/petertankov/green-invest.

Acknowledgments

We thank Frédéric Ghersi, Jean-Charles Hourcade and Stéphane Voisin for numerous insightful discussions.

This research was supported by ADEME (Agency for Ecological Transition), France and by Crédit Agricole S.A. in the context of SECRAET project, as well as by the FIME (Finance for Energy Markets) research initiative of the Institut Europlace de Finance. The sponsors played no role in the study.

References

Abadie, L.M., Chamorro, M., González-Eguino, M., 2011. Optimal abandonment of EU coal-fired stations. Energy J. 32 (3).

ACIL, 2014. Fuel and technology cost review – report to Australian energy market operator.

Bogdanov, D., Farfan, J., Sadovskaia, K., Aghahosseini, A., Child, M., Gulagi, A., Oyewo, A.S., Barbosa de Souza Noel Simas, L., Breyer, C., 2019. Radical transformation pathway towards sustainable electricity via evolutionary steps. Nature Commun. 10 (1), 1–16.

Boomsma, T.K., Meade, N., Fleten, S.-E., 2012. Renewable energy investments under different support schemes: A real options approach. European J. Oper. Res. 220 (1), 225–237.

Cronin, J., Anandarajah, G., Dessens, O., 2018. Climate change impacts on the energy system: A review of trends and gaps. Clim. Change 151 (2), 79–93.

Dalby, P.A., Gillerhaugen, G.R., Hagspiel, V., Leth-Olsen, T., Thijssen, J.J., 2018. Green investment under policy uncertainty and Bayesian learning. Energy 161, 1262–1281.

Detemple, J., Kitapbayev, Y., 2020. The value of green energy: Optimal investment in mutually exclusive projects and operating leverage. Rev. Financ. Stud. 33 (7), 3307–3347.

Flora, M., Vargiolu, T., 2020. Price dynamics in the European Union Emissions Trading System and evaluation of its ability to boost emission-related investment decisions. European J. Oper. Res. 280 (1), 383–394.

Fuss, S., Szolgayová, J., Khabarov, N., Obersteiner, M., 2012. Renewables and climate change mitigation: Irreversible energy investment under uncertainty and portfolio effects. Energy Policy 40, 59–68.

Hach, D., Spinler, S., 2016. Capacity payment impact on gas-fired generation investments under rising renewable feed-in—A real options analysis. Energy Econ. 53, 270–280.

International Energy Agency, 2020. Projected costs of generating electricity.

Laurikka, H., Koljonen, T., 2006. Emissions trading and investment decisions in the power sector—A case study in Finland. Energy Policy 34 (9), 1063–1074.

Longstaff, F.A., Schwartz, E.S., 2001. Valuing American options by simulation: A simple least-squares approach. Rev. Financ. Stud. 14 (1), 113–147.

McGlade, C., Ekins, P., 2015. The geographical distribution of fossil fuels unused when limiting global warming to 2°C. Nature 517 (7533), 187–190.

Mercure, J.-F., Pollitt, H., Viñuales, J.E., Edwards, N.R., Holden, P.B., Chewpreecha, U., Salas, P., Sognnaes, I., Lam, A., Knobloch, F., 2018. Macroeconomic impact of stranded fossil fuel assets. Nature Clim. Change 8 (7), 588–593.

Metz, B., Davidson, O., Bosch, P., Dave, R., Meyer, L. (Eds.), 2007. Contribution of Working Group III to the Fourth Assessment Report of the Intergovernmental Panel on Climate Change. Cambridge University Press, Cambridge, United Kingdom and New York, NY, USA.

Mo, J., Cui, L., Duan, H., 2021. Quantifying the implied risk for newly-built coal plant to become stranded asset by carbon pricing. Energy Econ. 99, 105286.

Rozenberg, J., Vogt-Schilb, A., Hallegatte, S., 2020. Instrument choice and stranded assets in the transition to clean capital. J. Environ. Econ. Manag. 100, 102183.

Siddiqui, A., Fleten, S.-E., 2010. How to proceed with competing alternative energy technologies: A real options analysis. Energy Econ. 32 (4), 817–830.

Stanton, M.C.B., Dessai, S., Paavola, J., 2016. A systematic review of the impacts of climate variability and change on electricity systems in Europe. Energy 109, 1148–1159.

Teske, S., 2019. Achieving the Paris Climate Agreement Goals: Global and Regional 100% Renewable Energy Scenarios with Non-Energy GHG Pathways for +1.5°C and +2°C. Springer, Nature.

Van der Ploeg, F., Rezai, A., 2020. The risk of policy tipping and stranded carbon assets. J. Environ. Econ. Manag. 100, 102258.

Welsby, D., Price, J., Pye, S., Ekins, P., 2021. Unextractable fossil fuels in a 1.5°C world. Nature 597 (7875), 230–234.